Genetic disorders in the growth hormone-IGF-I axis

Walenkamp, M.J.E.

Structural and functional characteristics of the Val^{44}Met IGF-I missense mutation: correlation with effects on growth and development

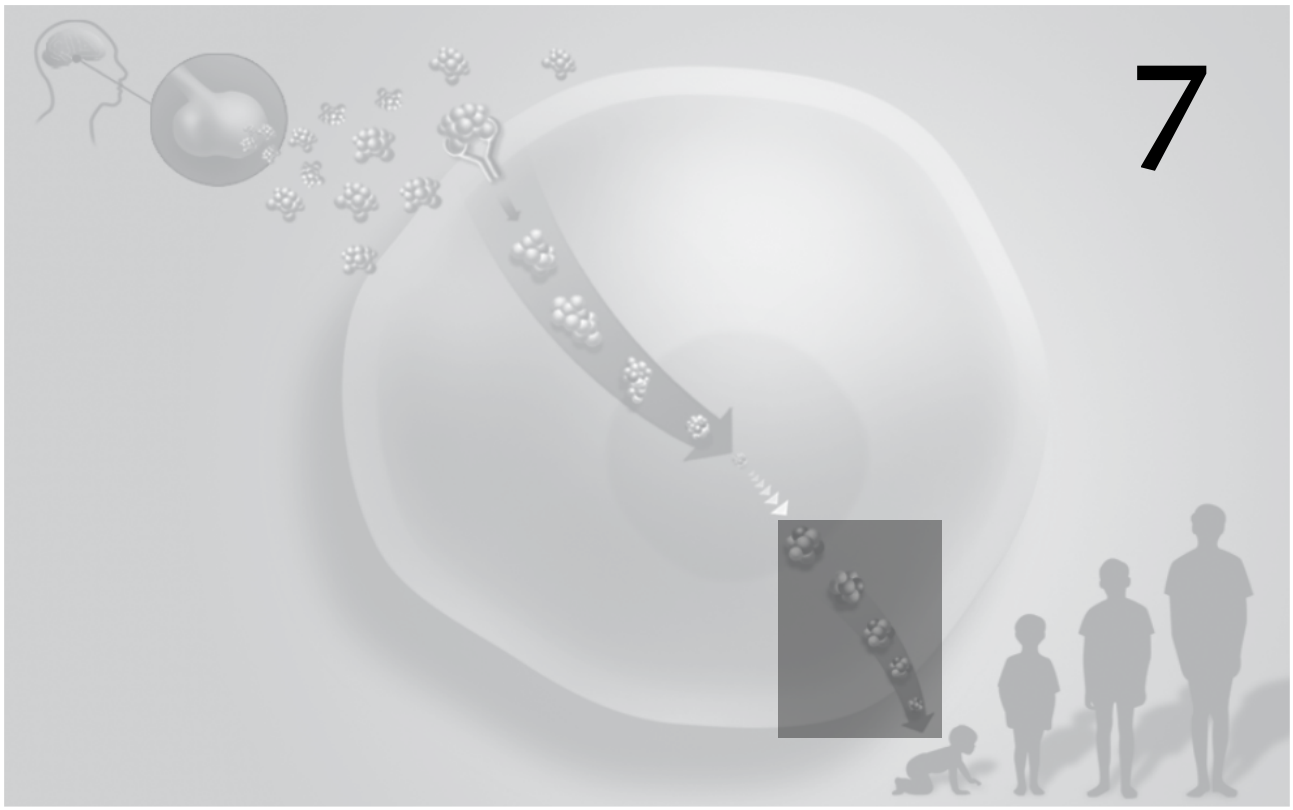

Adam Denley[1], Chunxiao C. Wang[2], Kerrie A. McNeil[1], Marie J. E. Walenkamp[3], Hermine A. van Duyvenvoorde[3], Jan M. Wit[3], John C. Wallace[1], Raymond S. Norton[2], Marcel Karperien[3,4], and Briony E. Forbes[1]

[1] School of Molecular and Biomedical Science, The University of Adelaide, Australia
[2] The Walter and Eliza Hall Institute of Medical Research, Victoria, Australia
[3] Department of Pediatrics, [4] Department of Endocrinology and Metabolic Diseases Leiden University Medical Center, Leiden, The Netherlands

Molecular Endocrinology 2005;19(3):711-721

Abstract

We have previously described the phenotype resulting from a missense mutation in the IGF-I gene, which leads to expression of IGF-I with a methionine instead of a valine at position 44 (Val^{44}Met IGF-I). This mutation caused severe growth and mental retardation as well as deafness evident at birth and growth retardation in childhood, but is relatively well tolerated in adulthood. We have conducted a biochemical and structural analysis of Val^{44}Met IGF-I to provide a molecular basis for the phenotype observed. Val^{44}Met IGF-I exhibits a 90-fold decrease in type 1 IGF receptor (IGF1R) binding compared with wild-type human IGFI and only poorly stimulates autophosphorylation of the IGF1R. The ability of Val^{44}Met IGF-I to signal via the extracellular signal-regulated kinase 1/2 and Akt/protein kinase B pathways and to stimulate DNA synthesis is correspondingly poorer. Binding or activation of both insulin receptor isoforms is not detectable even at micromolar concentrations. However, Val^{44}Met IGF-I binds IGF-binding protein 2 (IGFBP-2), IGFBP-3, and IGFBP-6 with equal affinity to IGF-I, suggesting the maintenance of overall structure, particularly in the IGFBP binding domain. Structural analysis by nuclear magnetic resonance confirms retention of near native structure with only local side-chain disruptions despite the significant loss of function. To our knowledge, our results provide the first structural study of a naturally occurring mutant human IGF-I associated with growth and developmental abnormalities and identifies Val^{44} as an essential residue involved in the IGF–IGF1R interaction.

Introduction

The IGF system plays an important role in normal growth and development. Activation of the type-1 IGF receptor (IGF1R) by IGF-I or IGF-II results in potentiation of growth, survival and differentiation. The action of IGFs is modulated by IGF binding proteins (IGFBPs), which regulate the availability to bind to the IGF1R.

The importance of IGF-I in normal growth has been demonstrated experimentally in mice with IGF-I knockout (1). These mice exhibit a deficiency in intrauterine growth, and those that survive continue to show restricted growth. At birth they are 60% of normal weight, but fall to 30% normal weight in adulthood (1, 2). The significance of IGF-I in normal growth is also demonstrated by disease states in which a disruption in circulating IGF-I levels occurs. Overexpression of IGF-I resulting from overproduction of GH leads to acromegaly, whereas low IGF-I levels resulting from an inactive GH receptor lead to Laron dwarfism (3, 4).

We have recently described the phenotype resulting from a homozygous missense mutation in the human IGF-I gene (5). The mutation (G274A) leads to the expression of IGF-I with a methionine instead of a valine at residue 44 (Val^{44}Met IGF-I). This was the first description of the effect of IGF-I deficiency in adulthood; the individual carrying the homozygous mutation is now 55 yr old. We observed several similarities between this individual and an earlier report of an IGF-I gene deletion described in a young male (6). Both patients suffered severe pre- and postnatal growth retardation, deafness and mental retardation. In adulthood, however, the lack of functional IGF-I is well tolerated, with effects mainly on bone mass and gonadal function (5).

In this study we describe biochemical and structural analysis of Val^{44}Met IGF-I and provide an explanation for the growth and developmental abnormalities observed. Native IGF-I is a single polypeptide chain of 70 amino acid residues, that contains three α-helical regions surrounding a hydrophobic core (7, 8). Residues 3-29 of IGF-I, which are homologous to the B chain of insulin, include helix 1 (Ala^{8}-Cys^{18}), and residues 42-60, which are homologous to the insulin A chain, include helices 2 (Ile^{43}-Cys^{48}) and 3 (Leu^{54}-Tyr^{60}). Residues 30-41 make up the C region loop, which is missing in insulin, and residues 61-70 make up the C-terminal D region

tail. We show that substitution of Met for Val at residue 44 of IGF-I results in a 90-fold reduced affinity for the IGF1R and a correspondingly lower activation of downstream signaling pathways. Remarkably, Val^{44}Met IGF-I binds with equal affinity to IGFBP-2, -3 and -6, suggesting maintenance of overall structure. This was confirmed by nuclear magnetic resonance analyses revealing only local side chain disruptions compared with IGF-I. Our study identifies Val^{44} as an essential residue involved in IGF-IGF1R interaction.

Results

Receptor binding [IGF1R and Insulin Receptor (IR)] and activation

Purified IGF-I and Val^{44}Met IGF-I were analyzed for their relative abilities to bind and activate the IGF1R and both isoforms of the IR (IR-A and IR-B). Competition binding curves for binding to the IGF1R are shown in Fig. 1A and 50% inhibitory concentration (IC_{50}) values are summarized in Table 1. As reported previously (5), the affinity of Val^{44}Met IGF-I is approximately 90-fold lower than that of IGF-I for the IGF1R. IGF1R activation on P6 cells was assessed using IGF-I, IGF-II, insulin and Val^{44}Met IGF-I (Fig. 1B). Although IGF-I activates the IGF1R with an IC_{50} of 3.9 ± 0.43 nM, IGF-II at the same concentration is only able to induce IGF1R phosphorylation equal to 35% that of IGF-I. In addition, activation of the IGF1R by insulin can only be detected at concentrations greater than 50 nM. Here we show that Val^{44}Met IGF-I is only slightly more potent than insulin in IGF1R activation as a result of decreased receptor binding affinity.

Competition binding curves for binding to the two isoforms of the IR (IR-A and IR-B) are shown in Fig. 2, and IC_{50} values are summarized in Table 2. No competition by Val^{44}Met IGF-I for europium-labeled insulin (Eu-insulin) binding is detected using either IR-A or IR-B, even at micromolar concentrations. IGF-I is a relatively poor binder to both IR isoforms and binds with a 3-fold higher affinity to the IR-A (IC_{50} = 120 nM) than to IR-B (IC_{50} = 366 nM). In contrast, insulin binds with high affinity to both IR isoforms, with a slightly higher affinity to the IR-B isoform in our assay (IR-A, IC_{50} = 1.4 nM ; IR-B, IC_{50} = 2.8 nM) (9). IGF-II also competes with high affinity (IC_{50} = 18nM) for Eu-insulin binding to the IR-A and has a 3.7-fold lower affinity for the IR-B. In addition, activation of the IR by concentrations of up

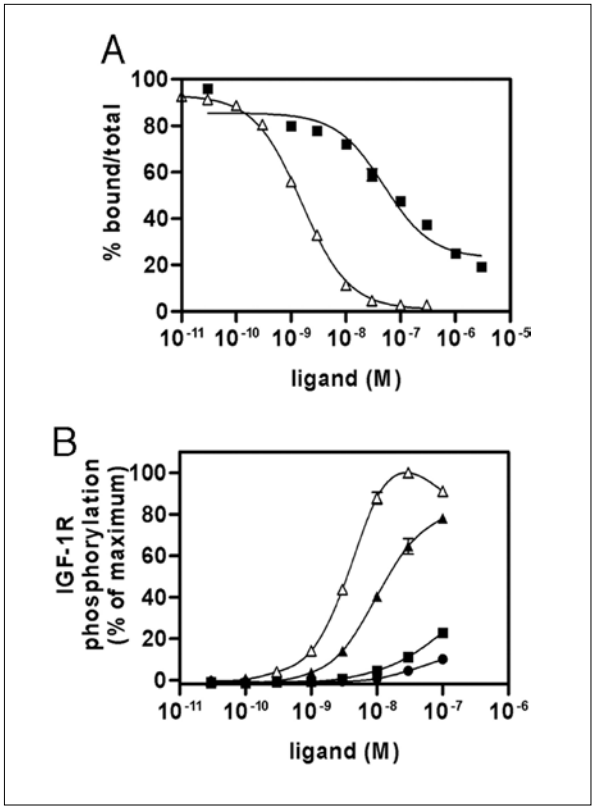

Figure 1. Binding and Activation of Human IGF1R by Val[44]Met IGF-I

A. Immunocaptured IGF1R was incubated with Eu-IGF-I in the presence or absence of increasing concentrations of IGF-I or Val[44]Met IGF-I as described in *Materials and Methods*. The graph shown is a representative of two independent experiments. Results are expressed as a percentage of Eu-IGF-I bound in the absence of competing ligand, and the data points are the mean ± SEM of triplicate samples. Errors are shown when they are greater than the size of the symbols. The ligands are as follows: A, IGF-I (Δ); Val[44]Met IGF-I (■);

B. IGF1R phosphorylation by IGF-I, IGF-II, insulin, and Val[44]Met IGF-I. P6 cells overexpressing the human IGF1R were serum-starved for 4 h, followed by stimulation with various concentrations of ligand for 10 min. Cells were lysed with ice-cold lysis buffer containing phosphatase inhibitors and activated receptors were immunocaptured with the anti-IGF1R antibody 24-31 as described in *Materials and Methods*. Receptor autophosphorylation was measured by time-resolved fluorescence using Eu-PY20 to detect phosphorylated tyrosines. The graph shown is a representative of three experiments and data points are the mean ± SEM of triplicate points. Errors are shown when they are greater than the size of the symbols. The ligands are as follows: B, IGF-I (△), IGF-II (▲), insulin (●), and Val[44]Met IGF-I (■).

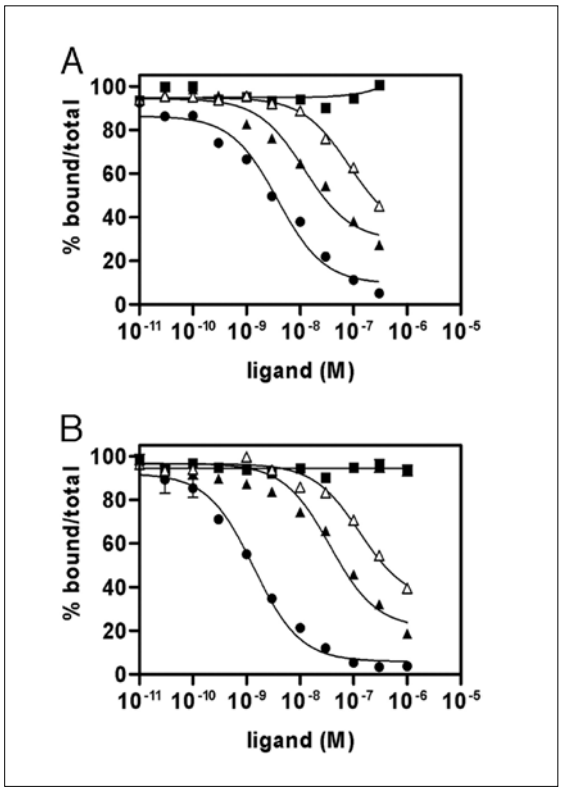

Figure 2. Competition Binding Curves of Eu-Insulin Binding to Immunopurified Human IR-A or IR-B. Immunocaptured IR-As or IR-Bs were incubated with Eu-insulin in the presence or absence of increasing concentrations of insulin, IGF-I, IGF-II, or Val^{44}Met IGF-I as described in *Materials and Methods*. The graphs shown are a representative of three experiments.

A. competition for binding to IR-A

B. competition for binding to the IR-B. Results are expressed as a percentage of Eu-insulin bound in the absence of competing ligand and the data points are the mean ± SEM of triplicate samples. Errors are shown when they are greater than the size of the symbols. The ligands are as follows in A and B, insulin (●); IGF-II (▲); IGF-I (△); Val^{44}Met IGF-I (■).

to 1 μM Val^{44}Met IGF-I is not detectable (data not shown), whereas the extent of IR phosphorylation by the other ligands correlates with receptor binding affinities (9).

In summary, IGF1R binding affinity of Val^{44}Met IGF-I is 90-fold lower than that of IGF-I and activation is correspondingly lower. IR binding and, therefore, activation are disrupted very significantly by substitution of valine for methionine at residue 44.

Table 1. Inhibition of Eu-IGF-I binding to the IGF1R by IGF-I and Val^{44}Met IGF-I

Ligand	IC_{50} (nM)	IC_{50} relative to IGF-I
IGF-I	1.7 ± 0.09	1
Val^{44}Met IGF-I	142 ± 43	83.8

The IC_{50} relative to that of IGF-I is also shown. Values are the mean ± SEM from two independent experiments.

Table 2. Inhibition of Eu—Insulin for binding to the IR-A and IR-B by insulin, IGF-I, IGF-II, and Val^{44}Met IGF-I

Ligand	IR-A		IR-B	
	IC_{50}(nM)	IC_{50} relative to IGF-I	IC_{50} (nM)	IC_{50} relative to IGF-I
IGF-I	120.4 ±34.1	1	366 ±15	1
Val^{44}Met IGF-I	>1000	ND	>1000	ND
Insulin	2.8 ±0.3	0.02	1.4±0.1	0.004
IGF-II	18.2 ±2.4	0.15	68 ±11	0.19

The IC_{50} relative to that of IGF-II binding to the IR-A is also shown. Values are the mean ± SEM from three independent experiments. ND, not determined.

Receptor signaling and biological activity in fibroblasts

To examine the effect of the Val^{44}Met-mutation on the ability to activate signal transduction in cells with a more physiological number of IGF1R, activation of the extracellular signal-regulated kinase 1/2 (Erk1/2) and Akt/protein kinase B (PKB) pathways was analyzed in cultures of dermal fibroblasts. After a 10-min stimulation by IGF-I or Val^{44}Met IGF-I, a dose-dependent activation of Erk1/2 was detected (Fig. 3). Approximately 100-fold more Val^{44}Met- IGF-I was required to induce detectable Erk1/2 phosphorylation. The maximal stimulation reached with Val^{44}Met IGF-I was about half of the activation level reached by IGF-I. In contrast, approximately 200-fold more Val^{44}Met IGF-I was required to activate Akt/PkB on Ser^{473} and Thr^{308} compared with IGF-I. Again, the maximal stimulation of Akt/PKB reached with Val^{44}Met IGF-I varied between 70% and 40% of the levels induced by IGF-I (Fig. 3). In summary, the reduced activation of downstream signaling by Val^{44}Met IGF-I corresponds with its reduced affinity for the IGF1R compared with

IGF-I. However, there appears to be a greater effect on signaling via the Akt/PKB pathway than on Erk1/2 signaling, indicating a differential ability to stimulate signaling outcome after binding by Val^{44}Met IGF-I.

Subsequently, the ability of Val^{44}Met IGF-I to stimulate DNA synthesis was measured in primary cultures of skin fibroblasts isolated from the patient and a normal age- and sex-matched subject. IGF-I was able to stimulate DNA synthesis in both the patient and the normal fibroblasts to a similar extent. In contrast, Val^{44}Met IGF-I was unable to stimulate DNA synthesis in either cell type in the

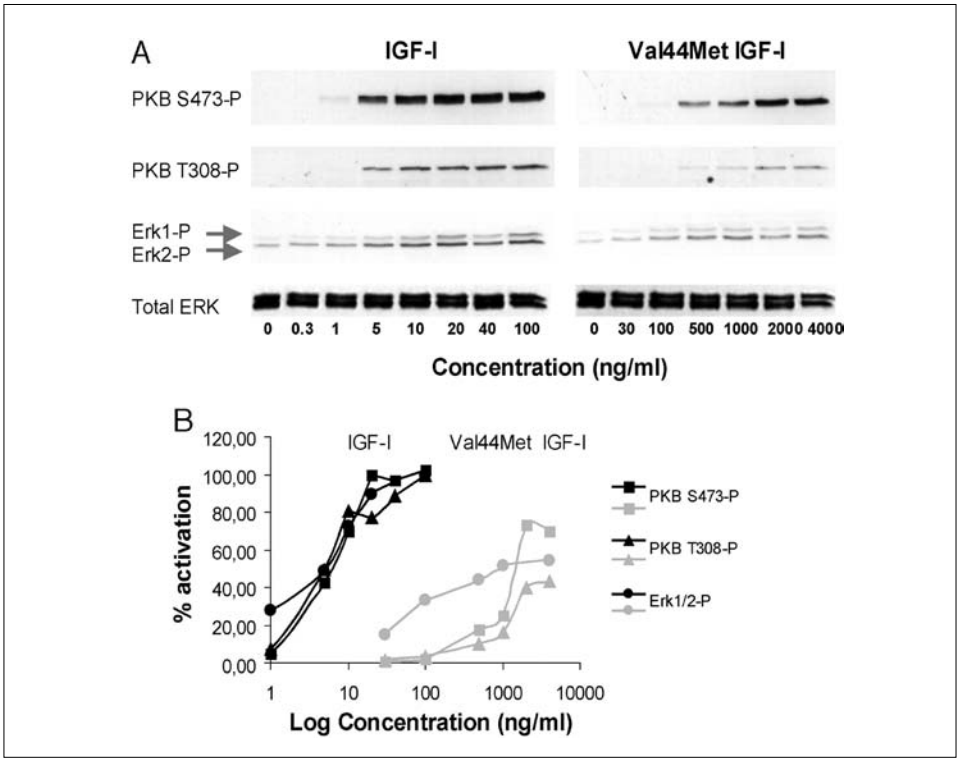

Figure 3. Activation of PKB/Akt and Erk1/2 in Skin Fibroblasts by Val^{44}Met IGF-I.

A. Western blot analysis of fibroblasts stimulated for 10 min with a dose-response range of IGF-I and Val^{44}Met IGF-I. The blots were probed with phospho-specific antibodies for activation of PKB at Ser^{473} and Thr^{308} and Erk1/2. Total Erk was used to check for equal loading. Pictures are a representative example of a duplicate experiment.

B. Quantification by densitometric scanning of the blots shown in A. Values were expressed as a percentage of the maximal activation level reached with IGF-I, which was set to 100%, and were corrected for loading efficiency using total Erk.

physiological dose-response range of IGF-I (1-100 ng/ml; Fig. 4). When 100-fold higher concentrations of Val[44]Met IGF-I were used (>1000 ng/ml), small inductions of [^{3}H]thymidine incorporation were observed, which leveled off at about 45% of the levels reached by IGF-I. These experiments indicate that the patient's IGF-1Rs were functioning normally, but the Val[44]Met IGF-I was unable to elicit a biological response in the normal dose-response range of IGF-I action.

IGFBP binding

We previously reported that neutral gel filtration of the patient's serum showed that endogenous Val[44]Met IGF-I predominantly associates with the 150-kDa complex (comprised of Val[44]Met IGF-I, IGFBP-3, and the acid labile subunit) as seen with wild type IGF-I in control serum (5). Additional IGFBP binding was assessed using BIAcore analysis with IGFBP-2, IGFBP-3 and IGFBP-6 biosensor surfaces (Fig. 5). There was no difference in binding affinities between IGF-I and Val[44]Met IGF-I for any of the surfaces. IGFBP-2 and IGFBP-3 exhibit similar affinities for IGF-I and Val[44]Met IGF-I (0.7 nM), whereas IGFBP-6 bound IGF-I and Val[44]Met IGF-I with a much lower affinity (6.6 nM; see Fig. 5). Because IGFBP binding was not perturbed we can conclude that Val[44]Met IGF-I is correctly folded.

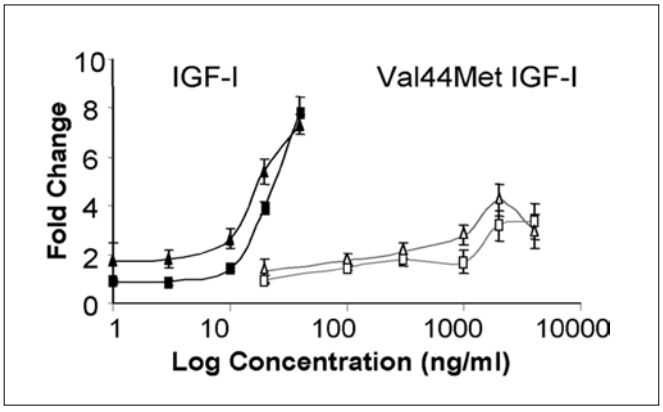

Figure 4. Stimulation of DNA synthesis in Normal and Patient Skin Fibroblasts by Val[44]Met IGF-I. Increasing concentrations of Val[44]Met IGF-I (*gray lines*) and IGF-I (*black lines*) were used to stimulate DNA synthesis in fibroblasts from the patient (△ and ▲) and a normal age- and sex-matched individual (□ and ■). Amount of incorporation of [^{3}H]thymidine is expressed as the fold change over that in unstimulated fibroblasts and represents the mean of a triplicate experiment ± SEM.

Structural analysis of Val^{44}Met IGF-I by NMR

To determine whether there were any significant structural differences between Val^{44}Met IGF-I and wild-type IGF-I, NMR spectra of mutant IGF-I were compared with those of the native protein (supplemental Fig. 1, published on The Endocrine Society's Journals Online web site at http://mend.endojournals.org). ^{1}H and ^{15}N NMR resonance assignments for Val^{44}Met IGF-I were made from a three-dimensional nuclear overhauser effect spectroscopy heteronuclear single quantum coherence (NOESY-HSQC) spectrum. The assignment process was assisted by comparison of two-dimensional ^{15}N-^{1}H HSQC spectra of Val^{44}Met IGF-I with those of IGF-I in the presence of excess IGF-F1-1 peptide (8), long-[Arg^{3}]IGF-I (10) and long-[Leu^{60}]IGF-I (11), although some significant discrepancies exist among the

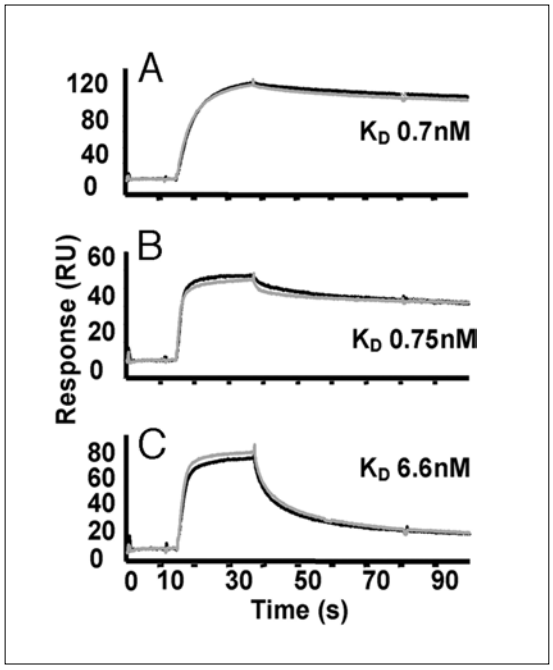

Figure 5. Surface Plasmon Resonance Analysis of Val^{44}Met IGF-I Binding to IGFBP-2, -3, and -6.
Sensorgrams represent binding to IGFBP-2 (A), IGFBP-3 (B), and IGFBP-6 (C) surfaces at 50 nM IGF-I (*black line*) or Val^{44}Met IGF-I (*gray line*). Kinetic studies with a range of analyte concentrations were determined at a flow rate of 40 µl/min to minimize mass transfer effects, allowing 300 sec for association and 900 sec for dissociation. Dissociation constants (K_d) were derived using BIAevaluation 3.2 software an a 1:1 Langmuir binding model.

assignments for these three proteins, as summarized in supplemental Table 1, published on The Endocrine Society's Journals Online web wite at http://mend.endojournals.org. One group of residues, including Cys^{6}, Gly^{7}, Leu^{10}, Val^{11}, Phe^{16}, Arg^{50}, and Leu^{54}, is affected by F1 peptide binding to IGF-I (8), so their chemical shifts differed from those of Val^{44}Met IGF-I, long-[Arg^{3}] IGF-I and long-[Leu^{60}] IGF-I. A second group, including Ala^{8}, Phe^{25}, Ile^{43}, Ser^{51}, Arg^{55}, and Tyr^{60}, differed in the Val^{44}Met IGF-I mutant as a direct consequence of the mutation. Resonances from Gly^{7}, Leu^{10}, Glu^{58}, and Cys^{61} were not found in spectra of Val^{44}Met IGF-I even at lower temperatures (15° and 20°C).

Chemical shift differences between Val^{44}Met IGF-I and IGF-I were small, except for Cys^{6}, Ala^{8}, Phe^{23}, Ile^{43}, Asp^{45}, Ser^{51}, Arg^{56}, Leu^{57} and Tyr^{60} (Fig. 6). The largest changes were for Ile^{43} and Asp^{45}, which flank the site of substitution, and Arg^{56}, which is located in the middle of second helix of the A region, about 9.1-11.2 Å away from Val^{44} (NH-NH distance) in the long-[Arg^{3}]IGF-I structure (12) and 11.5-12.6 Å away in the IGF-I plus F1 peptide structure (8). Two of the residues strongly affected, Phe^{23} and Tyr^{60}, are implicated in IGF-I binding to IGF1R (13, 14) (Fig. 7). Thus, although the structure of Val^{44}Met IGF-I is similar to that of native, chemical shift comparisons suggest that the mutation has caused local structural changes around the mutant site and in surrounding regions, some of which are involved in binding to the IGF-I receptor

This conclusion is supported by a detailed analysis of nuclear overhauser effects (NOEs) from the backbone amide resonances. If the distance between two protons is less than 6 Å in the structure, an NOE between those two protons should be observable in NMR spectra. Most of the observed NOEs to Met^{44} (Table S2) are consistent with the native structure, although the NOE between Met^{44} H and Thr^{41} NH is new, suggesting that the side-chain of Met^{44} has a different orientation from that of Val^{44} in native IGF-I. The relative intensities of the backbone NOEs to Met^{44} in Val^{44}Met IGF-I indicate that the native helix encompassing residues 43-48 is maintained, with HN-HN NOEs from Met^{44} to Ile^{43} and Asp^{45} being observed, as expected for an α-helix (15). One difficulty in making a detailed comparison with native IGF-I is that neither of the two high-quality solution structures for IGF-I corresponds precisely to IGF-I. Long-[Arg^{3}]IGF-I has a substitution at position 3 and an N-terminal extension (although this is not shown in Fig. 7), and the other has a peptide from phage display bound to it (again, not shown in Fig. 7). It is clear

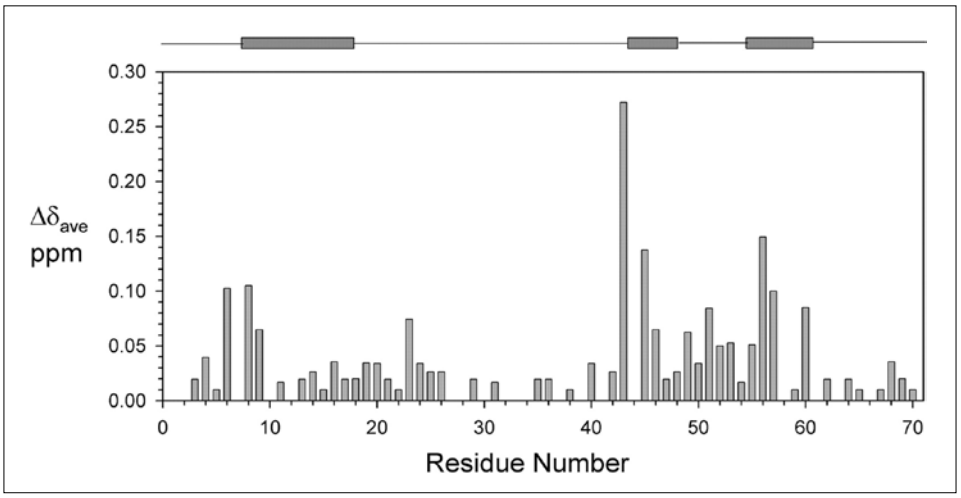

Figure 6. Weighted Average Chemical Shift Differences between Val[44]Met IGF-I and Native IGF-I
The average chemical shift differences derived from our spectra were calculated for ^{15}N and ^{1}H resonances using $\Delta\delta_{av} = (\Delta\delta_{NH}^2 + 0.17\Delta\delta_N^2)^{1/2}$(66). Residues Gly[1], Gly[7], Leu[10], Glu[58], and Cys[61] were not assigned. Residues 2, 28, 39, 63 and 66 are proline and Asp[12], Lys[27], Gly[30], Gly[32], Ser[33], Ser[34], Arg[37], and Thr[41] had zero $\Delta\delta_{av}$ values. The locations of the three helices of native IGF-I are indicated above the plot.

from Fig. 7 that these structures are not identical. From inspection of the pattern of chemical shift perturbations and NOEs observed for Val[44]Met, it appears that the structure of long-[Arg[3]]IGF-I may be more representative of Val[44]Met.
Deviations from random coil chemical shifts for backbone ^{15}N, NH, and H^{α} resonances are a valuable indicator of ordered secondary structure in proteins (16). These plots for Val[44]Met IGF-I (Fig. S2) are consistent with the secondary structure of native IGF-I. Plots of ^{15}N backbone relaxation parameters R_1, R_2, and NOE for Val[44]Met IGF-I as a function of residue number (Fig. S3) are similar to those for long-[Arg[3]]IGF-I (12), with the regions of ordered secondary structure showing positive NOEs and faster spin-spin relaxation (larger R_2 values) and the N- and C-termini and the C region having smaller NOEs (in some cases negative) and smaller R_2 values. The mean R_1, R_2 and NOE values for Val[44]Met IGF-I are 1.40 ± 0.12 s^{-1}, 10.05 ± 0.46 s^{-1}, and 0.42 ± 0.02, respectively, compared with values of approximately 1.39 s^{-1}, 7.69 s^{-1} and 0.55 ± 0.12, respectively, in long-[Arg[3]]IGF-I. Detailed comparisons are difficult because of differences in protein concentration and state

of aggregation, but one significant difference between the two data sets occurs at residues 52 and 53, which have low NOEs and smaller R_2 values in Val[44]Met IGFI than long-[Arg[3]]IGF-I. This suggests that the loop connecting helices 2 and 3 in the native structure (arrowed in Fig. 7) may be somewhat more flexible in Val[44]Met.

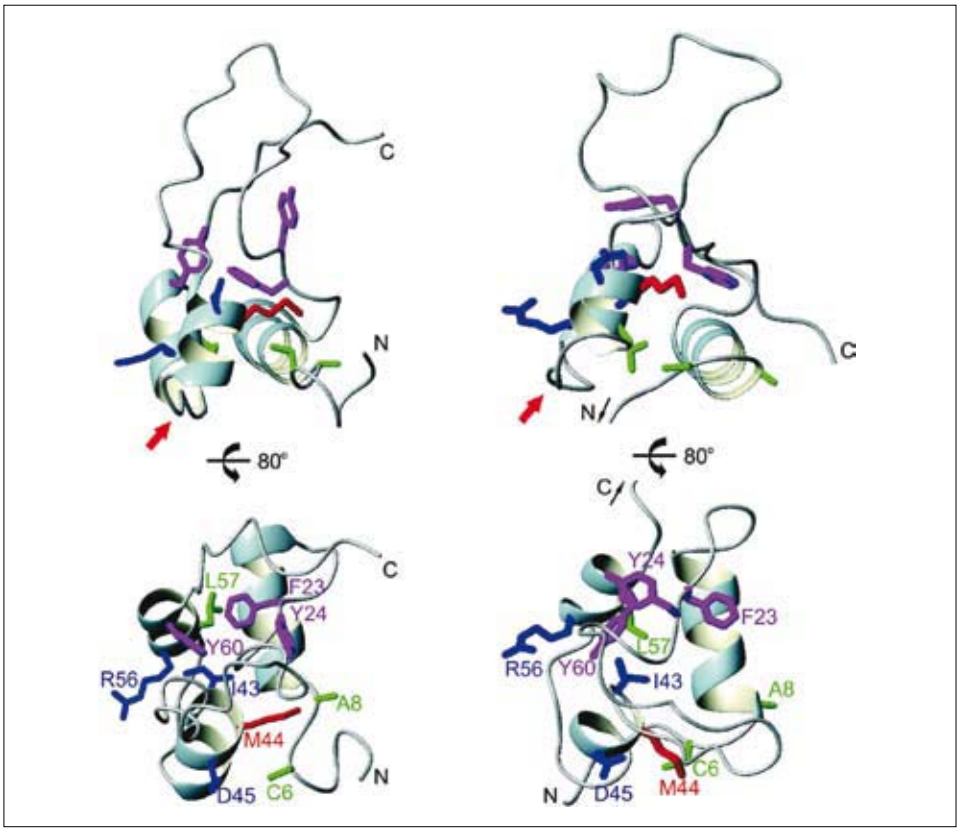

Figure 7. Backbone Ribbon View of IGF-I with Side-Chains of Key Residues Indicated
Long-[Arg[3]] IGF-I (12) (PDB accession no. 3LRI) is shown on the *left*, and IGF-I + F1 peptide (8) (PDB accession no. 1PMX) is shown on the *right* (with the peptide not shown for clarity); in each case the closest to average structure over the family is shown. Side chains are colored as follows: Met[44] in *red*; Ile[43], Asp[45], and Arg[56], which have the largest chemical shift changes between mutant and native IGF-I, in *blue*; Cys[6], Ala[8], and Leu[57], which have smaller chemical shift changes between mutant and native IGF-I, in *green*, and Phe[23], Tyr[24], and Tyr[60], which are implicated in IGF-I binding to the type 1 IGF receptor (13, 22, 27, 67) in *magenta*. The *upper* and *lower* views of each structure are related by an 80° rotation around the horizontal axis. The loop connecting helices 2 and 3 in the native structure is *arrowed*; note that the last five residues in the *lower* view of IGF-I + F1 peptide, and the first two residues in the *upper* view, are not shown in order to avoid overlap. The N-terminal extension in long-[Arg[3]]IGF-I is not shown, so the chain begins at the equivalent of Gly[1] of IGF-I.

Discussion

We have conducted a comprehensive biochemical and structural analysis of Val^{44}Met IGF-I in order to explain the phenotype described of a patient carrying a point mutation in the IGF-I gene. A similar phenotype was previously described resulting from a deletion in the IGF-I gene (6). The phenotype is not due to a defective IGF1R as IGF-I can stimulate the same biological response in fibroblasts derived from the patient or from a normal individual. However, we demonstrate that the Val^{44}Met mutation results in a significant reduction (~90-fold) in IGF1R receptor binding affinity and undetectable binding to either IR isoform. As a consequence, phosphorylation of the IGF1R and downstream-acting signaling proteins, *i.e.* Erk1/2 and Akt/PKB, is diminished. Remarkably, Val-Met substitution at position 44 seems to affect the Akt/PKB pathway to a greater extent than one would expect on the basis of receptor binding affinities. It is possible that these differences are a direct consequence of the changed kinetics of receptor-ligand interaction, which may have a greater impact on activation of the PKB/Akt-pathway than on the Erk1/2 pathway. This interesting finding is the subject of ongoing investigations.

Despite a large effect on receptor binding Val^{44}Met IGF-I is still able to bind IGFBP-2, IGFBP-3, and IGFBP-6 with equal affinity to IGF-I. This suggests that the common IGFBP-binding site is not disrupted. In support of this conclusion we see that Val^{44}Met IGF-I shows a normal association with the 150-kDa complex in serum (5). Dubaquie and Lowman (17) reported a small disruption in IGFBP-1 and IGFBP-3 binding by Val^{44}Ala IGF-I (2.3- and 1.4-fold lower binding than IGF-I, respectively), but did not report IGF1R binding. A recent crystal structure of IGF-I in complex with the N domain of IGFBP-5 shows that Val^{44} is not included in the N domain binding site (18). Headey *et al*. (19) reported that binding of IGFBP-6 C domain to IGF-II affects the two residues adjacent to Val^{43}, namely Ile^{42} and Glu^{44}. Although Val^{43} could not be assessed because of peak overlap, it seems that this region of the IGF-II surface is involved in interaction with the C domain of IGFBPs. Therefore, the lack of effect of the Val^{44}Met substitution in IGF-I on IGFBP binding may be attributable to the fact that the hydrophobic nature of the surface is preserved. The C domain of the IGFBPs is apparently less sensitive to the nature of the side-chain at position 44 than is the IGF-I receptor.

Interestingly, the results of the NMR analysis of the Val^{44}Met IGF-I structure suggest relatively little disruption of the overall structure. The marked effect on IGF1R binding could be explained by either local structural disruption around the mutation site and in surrounding areas or by a direct interaction of Val^{44} with the receptor. Analysis of chemical shift comparisons shows differences in local structure at residues Cys^{6}, Ala^{8}, Phe^{23}, Ile^{43}, Asp^{45}, Ser^{51}, Arg^{56}, Leu^{57}, and Tyr^{60}. Of these residues, Tyr^{60} has previously been implicated as important for IGF1R and IR binding (13, 20). Tyr^{60}Leu IGF-I has a 20-fold reduction in IGF1R binding affinity and Tyr^{60}Phe IGF-I has 2.6-fold reduced IR binding affinity. In addition, Maly and Luthi (21) showed that Tyr^{60} was protected from iodination in the presence of the IGF1R. Interestingly, iodination experiments with Val^{44}Met IGF-I revealed an approximately 10-fold reduced incorporation of ^{125}I compared with wild type (data not shown). These iodinations predominantly occur on tyrosine residues including Tyr^{60}. Reduced incorporation of ^{125}I is compatible with the local differences in structure at Tyr^{60}, which could make this residue less accessible for iodination. Phe^{23} has also been identified as important for IGF1R binding as mutation to Gly results in a 48-fold reduction in receptor binding affinity compared with IGF-I (14). Whether this mutation is causing a structural perturbation has not been investigated. The neighboring residue, Tyr^{24}, has been identified in several studies as being important for IGF1R binding (22). We have also previously demonstrated decreased IGF1R binding (~ 6-fold) by mutation of Ala^{8} to Leu (23). Only relatively small effects of mutating Ser^{51} and Arg^{5}6 have been reported (24, 25).

Val^{44} is conserved in all but one (catfish brain)(26) of the IGF-I sequences reported to date and is also found in the corresponding position in the two structurally related proteins, IGF-II and insulin. Interestingly, mutation of Val^{43} of IGF-II (which corresponds to Val^{44} in IGF-I) to Leu results in a 220-fold lower IGF1R binding affinity while maintaining IGFBP binding affinities similar to IGF-II (27). This observation confirms the importance of this residue in maintaining IGF1R binding.

A point mutation in the insulin gene (guanine to thymine at position 1298) resulting in the Val^{A3} to Leu mutation in the A chain has been termed insulin Wakayama (28, 29). Val^{A3} corresponds to Val^{44} of IGF-I. The expression of Val^{A3}Leu insulin leads to hyperinsulinemia and in some cases diabetes (29) resulting from severely defective IR binding. It has been suggested that Val^{A3} and Ile^{A2} make direct contact with the IR

after a structural change in insulin (30). Removal of contact between the beginning of the A chain and the C terminus of the B chain (involving residue B24) exposes residues Ile^{A2} and Val^{A3} and thereby allows their interaction with the IR (30-34). Substitution of Ile^{A2} with *allo*-Ile^{A2} leads to a 50-fold reduction in IR binding affinity while maintaining overall structure (32). Direct evidence for interaction with the receptor has recently been provided by a cross-linking study using a *p*-azido-Phe derivative of Val^{A3} and suggests an interaction with the insert domain (35).

Several substitutions have been made at Val^{A3} including Val^{A3}Leu insulin, which has only 0.14% of IR binding affinity compared with insulin (29, 36). Nakagawa and Tager (37) reported a similar helical content in Val^{A3}Leu insulin and native insulin after circular dichroism spectral analysis. Interestingly, NMR analysis of Val^{A3}Leu insulin revealed no significant change in structure (Weiss, M., unpublished observations) despite the significant effect on IR binding (29, 36). Structural analyses of Val^{A3}Ile (37) and Val^{A3}Thr (38) by far ultraviolet light circular dichroism show little disruption to the overall structure, whereas mutation to Gly leads to a complete disruption of the first A chain α-helix, as shown by NMR analysis (39). Furthermore, substitutions at residue Ile^{A2} highlight the importance of the beginning of the A domain helix in IR binding. Substitution of Ile^{A2} with Val reduces the helical content and destabilizes the first A domain helix (40). As with Val^{A3}Leu insulin (37), our data show that Val^{44}Met IGF-I maintains all helical structures. This is perhaps not surprising, because Met is a residue of reasonable helical propensity (41, 42) and is commonly found in the same position in proteins as Val (43). However, we did find that the loop connecting helices 2 and 3 in the native structure (Fig. 7) is somewhat more flexible in Val^{44}Met IGF. Despite this minor structural perturbation, both Val^{44}Met IGF-I and Val^{A3}Leu insulin have severely disrupted receptor binding properties. It seems likely that Val^{44} in IGF-I plays a similar role in IR binding to Val^{A3} in insulin.

In conclusion, we describe a biochemical and structural analysis of the first naturally occurring mutant of IGF-I. The mutant, Val^{44}Met IGF-I, exhibits large reductions in IGF1R and IR binding affinities and correspondingly lower potential to activate signaling events downstream of the IGF1R, while preserving native affinity to several binding proteins. Biological activities of Val^{44}Met IGF-I are only observed when supraphysiological concentrations (at least 100-fold higher) are used. In

the normal physiological dose-response range Val^{44}Met substitution is completely inactivating. These data led us conclude that the homozygous patient with the Val^{44}Met substitution is effective null for IGF-I. This fully explains the phenotype of our patient, and is in line with the observed similarities in developmental defects observed in our patient and in one previously described adolescent man with a homozygous IGF-I gene deletion, as well as in IGF-I knockout mice (1, 6). The lack of binding to the IR by Val^{44}Met IGF-I probably plays a minor role in the overall phenotype of our patient, because the affinity of IGF-I for either the IR-A or IR-B isoform is relatively low compared with that of insulin. Our structural analyses reveal only minor perturbations in the local structure of residues known to be involved in IGF1R binding and the overall structure is remarkably well preserved. Finally, our analysis identifies Val^{44} as a critical residue involved in receptor-ligand interactions, and further mutational analysis of this residue could provide valuable insight into the mechanism of IGF1R binding by IGF-I.

Materials and Methods

Materials

Oligonucleotides were purchased from Geneworks Pty Ltd. (Adelaide, Australia). Restriction enzymes were from New England Biolabs (Hitchin, UK) or Geneworks Pty Ltd. (Adelaide, Australia). ^{15}N-Labeled NH_4Cl was purchased from Sigma-Aldrich Corp. (Castle Hill, Australia). Human IGF-I for Eu labeling and human IGFBP-2 were purchased from GroPep Pty. Ltd. (Adelaide, Australia). Human IGFBP-3 and IGFBP-6 were from R&D systems (Minneapolis, MN). Human insulin was purchased from Novo Nordisk (Bagsværd, Denmark). Greiner Lumitrac 600 96-well plates were obtained from Omega Scientific (Tarzana, CA). DELFIA Eu labeling kit, DELFIA enhancement solution, and Eu-conjugated antiphosphotyrosine antibody PY20 were purchased from Perkin Elmer (Turku, Finland). Eu-IGF-I and Eu-insulin were produced as described by Denley *et al*. (9) according to the manufacturer's instructions.

Antibodies 83-7 and 24-31 were gifts from Prof. K. Siddle (Cambridge, UK). P6 cells (BALB/c3T3 cells overexpressing human IGF1R) (44) and R$^-$ cells (mouse 3T3-like cells with a targeted ablation of the IGF1R gene) (45) were gifts from Prof. R.

Baserga (Philadelphia, PA). Cells overexpressing the exon 11^-/IR-A and exon 11^+/IR-B isoforms of the IR (R^-IR-A and R^-IR-B cells, respectively) were created as previously described (9). Total Erk1/2, Phospho-p44/42 MAPK, Phospho-Akt (Ser^{473}) and Phospho-Akt (Thr^{308}) antibodies were obtained from Cell Signaling Technology (Beverly, CA).

Construction of expression plasmids encoding human IGF-I and Val^{44}Met IGF-I

Human IGF-I expression vector was developed by King *et al*. (46). The Quikchange site-directed mutagenesis kit was used to incorporate a G to A mutation in the IGF-I coding sequence at position 130 using the following oligonucleotides: Val^{44}Met forward 5' CCG CAG ACC GGA ATC ATG GAT GAA TGC TGC 3', Val^{44}Met reverse 5' GCA GCA TCC ATC CAT GAT TCC GGT CTG CGG 3'. The Val^{44}Met IGF-I-coding sequence was then subcloned using *Hpa*I and *Hind*III restriction enzymes into the pGH (1-11) expression vector (46).

Recombinant IGF-I and Val^{44}Met IGF-I production

IGF-I and Val44Met IGF-I were expressed and purified essentially as described by Shooter et al. (23). ^{15}N labeled Val^{44}Met IGF-I was expressed in minimal medium supplemented with ^{15}N-labeled NH_4Cl essentially as described previously (47). The purified proteins were analyzed by mass spectroscopy and N-terminal sequencing and were shown to have the correct masses (93% incorporation of ^{15}N) and to be greater than 95% pure. Quantitation of proteins was performed by comparing analytical C4 HPLC profiles with profiles of standard long-[Arg^3]IGF-I preparations (48).

Binding analysis of Val^{44}Met IGF-I to the IGF1R and IR isoforms

Receptor binding affinities were measured using an assay similar to that described for analyzing epidermal growth factor binding to the epidermal growth factor receptor (49) and outlined by Denley *et al*. (9). Briefly, R^-IR-A, R^-IR-B or P6 cells were lysed with lysis buffer (20 mM HEPES, 150 mM NaCl, 1.5 mM $MgCl_2$, 10% (vol/vol) glycerol, 1% (vol/vol) Triton X-100, 1 mM EGTA, 1mM phenylmethylsulfonylfluoride, pH 7.5) for 1 h at 4°C. Lysates were centrifuged for 10 min at 3500 rpm at 4°C, then 100 µl were added per well to a white Greiner Lumitrac 600 plate previously coated with anti-IR antibody 83-7 (50) or anti-IGF1R antibody 24-31 (51). Approximately 100,000 fluorescent counts of Eu-insulin or Eu-IGF-I

were added to each well along with various amounts of unlabeled competitor and incubated for 16 h at 4°C. Wells were washed with 20 mM Tris, 150 mM NaCl, and 0.05% (vol/vol) Tween 20 (TBST) and DELFIA enhancement solution (100 µl/well) was added. Time-resolved fluorescence was measured using 340-nm excitation and 612-nm emission filters with a BMG Lab Technologies Polarstar Fluorometer (Mornington, Australia).

IR and IGF1R phosphorylation assays

Receptor phosphorylation was detected essentially as described by Denley *et al*. (9). R$^-$IR-A, R$^-$IR-B cells or P6 cells (2.5 x 10^4 cells/well; Falcon 96-well, flat-bottom plate) were washed for 4 h in serum-free medium before treating with IGF-I, IGF-II, insulin or Val^{44}Met-IGF-I in 100µl DMEM with 1% BSA for 10 min at 37°C, 5% CO_2. Lysis buffer containing 2 mM Na_3VO_4 and 1 mg/ml NaF was added to cells, and receptors from lysates were captured on 96-well plates pre-coated with antibody 83-7 or 24-31 and blocked with 1x TBST/0.5% BSA. After overnight incubation at 4°C, the plates were washed with 1 x TBST. Phosphorylated receptor was detected with Eu-antiphosphotyrosine antibody PY20 (10 ng/well; room temperature, 2 h). DELFIA enhancement solution (100 µl/well) was added and time-resolved fluorescence was detected as described above.

Cell culture, [^{3}H]thymidine incorporation assay, and Western blot

[^{3}H]Thymidine incorporation assays and Western blotting were performed using fibroblast cultures, which were established from skin biopsies of the patient and an age- and sex-matched normal subject, as described in detail previously (52, 53).

BIAcore analysis of IGFBP binding

Coupling of IGFBPs to CM5 BIAsensor chips via amine group linkage was achieved using standard coupling procedures (54-56). Briefly, IGFBPs were coupled to activated surfaces (2 µg IGFBP/210 µl in 10 mM sodium acetate, pH 4.5) at 5 µl/min. Unreacted groups were inactivated with 35 µl 1 M ethanolamine-HCl, pH 8.5. A sensor surface with 600 response units (RU) coupled IGFBP-2 would routinely result in a response of approximately 100 RU with 100 nM IGF-I. In addition, a surface with 470 RU IGFBP-6 would result in a response of 70 RU, and a surface with 400 RU IGFBP-3 would result in a response of 45 RU with 100 nM IGF-I. Kinetic studies with 6.25, 12.5, 25, 50, and 100 nM IGF-I or Val^{44}Met IGF-I were

determined at a flow rate of 40 µl/min to minimize mass transfer effects and by allowing 300 sec for association and 900 sec for dissociation. IGFBP biosensor surfaces were regenerated with 10 mM HCl. Analysis of kinetic data was performed with BIAevaluation 3.2 software (Uppsala, Sweden). For each binding curve, the response obtained using control surfaces (no protein coupled) was subtracted. IGF-I binding fitted a 1:1 Langmuir binding model using global fitting. This model describes a simple reversible interaction of two molecules in a 1:1 complex. Goodness of fit measured as a χ^2 value was not greater than 5 for all experiments. All binding experiments were repeated at least in duplicate, and biosensor chips coupled at different times yielded surfaces with identical binding affinities. The binding affinities of IGF-I to IGFBP-2 (K_d = 0.7 nM), IGFBP-3 (K_d = 0.75 nM), and IGFBP-6 (K_d = 6.6 nM) were comparable to the binding affinities reported by Hobba *et al*. (57) and Wong *et al*. (58) for bovine IGFBP-2 (K_d = 0.3 nM) and human IGFBP-2 (K_d = 0.45 nM) respectively, Heding *et al*. (59) for IGFBP-3, (K_d = 0.23 nM), and were 5-fold higher than those of Marinaro *et al*. (60) for IGFBP-6 (K_a = 0.028 nM^{-1}) using BIAcore technology.

NMR structural analysis

Lyophilized, uniformly ^{15}N-enriched Val^{44}Met IGF-I was dissolved in 95% H_2O / 5% ^2H_2O containing 10 mM sodium acetate-$^2H_4$ and 0.02 % sodium azide. The protein concentration was approximately 0.9 mM, and the pH was adjusted to 5.1 without correcting for the deuterium isotope effect. The after-spectra were recorded at 37°C on a DRX-600 spectrometer (Bruker, Karlsruhe, Germany) using a triple-resonance probe equipped with triple-axis gradients: two-dimensional ^1H-^{15}N-HSQC, three-dimensional ^1H-^{15}N-NOESY-HSQC with a 150 msec mixing time, and ^{15}N T_1, T_2, and NOE measurements. A series of ^1H-^{15}N-HSQC spectra was recorded at temperatures of 15, 20, and 37°C on a Bruker Avance500 spectrometer equipped with a cryoprobe. Two-dimensional ^1H-^{15}N-HSQC and three-dimensional ^1H-^{15}N-NOESY-HSQC spectra were also run at 600 MHz and 37°C on native IGF-I (0.5 mM, pH 4.9, in 95% H_2O/5% ^2H_2O containing 10 mM sodium acetate). Water was suppressed using the Watergate pulse sequence (61). All spectra were processed in XWINNMR, version 3.5 (Bruker) and analyzed with XEASY, version 1.4 (62). ^1H chemical shifts were referenced to sodium 4,4-dimethyl-4-silapentane-1-sulphonate at 0 ppm via the H_2O signal, and ^{15}N chemical shifts were referenced indirectly using the $^{15}N/^1H$ &ratios (63). ^{15}N relaxation rates R_1 and R_2

were determined by fitting these measured peak intensities, respectively, to three- and two-parameter single-exponential decay curves using the program CURVEFIT (64). Steady-state ^{1}H-^{15}N NOE values were calculated from peak intensity ratios obtained from spectra acquired in the presence and absence of proton saturation. The SD of NOE values was determined from the background noise level of the spectra as described by Farrow *et al*. (65).

Acknowledgments

We thank Dr. Shenggen Yao (WEHI, Melbourne, Australia) for help with the NMR experiments, Dr. D.M. Ouwens and Prof. Dr. J.A. Maassen (Department of Molecular Cell Biology, Leiden University Medical Center, Leiden, The Netherlands) for helpful discussions on Western blot analysis, and Dr. Jaap van Doorn (Department of Metabolic and Endocrine Diseases, University Medical Center Utrecht, Utrecht, The Netherlands) for critical reading the manuscript.

References

1. Liu JP, Baker J, Perkins AS, Robertson EJ, Efstratiadis A. Mice carrying null mutations of the genes encoding insulin-like growth factor I (Igf-1) and type 1 IGF receptor (Igf1r). Cell 1993;75(1):59-72.
2. Baker J, Liu JP, Robertson EJ, Efstratiadis A. Role of insulin-like growth factors in embryonic and postnatal growth. Cell 1993;75(1):73-82.
3. Baumann G. Genetic characterization of growth hormone deficiency and resistance: implications for treatment with recombinant growth hormone. Am J Pharmacogenomics 2002;2(2):93-111.
4. Paisley AN, Trainer PJ. Medical treatment in acromegaly. Curr Opin Pharmacol 2003;3(6):672-677.
5. Walenkamp MJ, Karperien M, Pereira AM, Hilhorst-Hofstee Y, Van Doorn J, Chen JW et al. Homozygous and heterozygous expression of a novel insulin-like growth factor-I mutation. J Clin Endocrinol Metab 2005;90(5):2855-2864.
6. Woods KA, Camacho-Hubner C, Savage MO, Clark AJ. Intrauterine growth retardation and postnatal growth failure associated with deletion of the insulin-like growth factor I gene. N Engl J Med 1996;335(18):1363-1367.
7. Brzozowski AM, Dodson EJ, Dodson GG, Murshudov GN, Verma C, Turkenburg JP et al. Structural origins of the functional divergence of human insulin-like growth factor-I and insulin. Biochemistry 2002;41(30):9389-9397.
8. Schaffer ML, Deshayes K, Nakamura G, Sidhu S, Skelton NJ. Complex with a phage display-derived peptide provides insight into the function of insulin-like growth factor I. Biochemistry 2003;42(31):9324-9334.
9. Denley A, Bonython ER, Booker GW, Cosgrove LJ, Forbes BE, Ward CW et al. Structural determinants for high-affinity binding of insulin-like growth factor II to insulin receptor (IR)-A, the exon 11 minus isoform of the IR. Mol Endocrinol 2004;18(10):2502-2512.
10. Laajoki LG, Le Breton E, Shooter GK, Wallace JC, Francis GL, Carver JA et al. Secondary structure determination of 15N-labelled human Long-[Arg-3]-insulin-like growth factor 1 by multidimensional NMR spectroscopy. FEBS Lett 1997;420(1):97-102.
11. Laajoki LG, Milner S, Francis G, Carver J, Keniry M. BioMagResBank (www.bmrb.wisc.edu/).0 1998;entry 4278.
12. Laajoki LG, Francis GL, Wallace JC, Carver JA, Keniry MA. Solution structure and backbone dynamics of long-[Arg(3)]insulin-like growth factor-I. J Biol Chem 2000;275(14):10009-10015.
13. Bayne ML, Applebaum J, Chicchi GG, Miller RE, Cascieri MA. The roles of tyrosines 24, 31, and 60 in the high affinity binding of insulin-like growth factor-I to the type 1 insulin-like growth factor receptor. J Biol Chem 1990;265(26):15648-15652.
14. Hodgson DR, May FE, Westley BR. Involvement of phenylalanine 23 in the binding of IGF-1 to the insulin and type I IGF receptor. Regul Pept 1996;66(3):191-196.
15. Wuthrich K. NMR of proteins and nucleic acids. New York: Wiley & Sons, 1986.
16. Wishart DS, Sykes BD. Chemical shifts as a tool for structure determination. Methods Enzymol 1994;239363-392.
17. Dubaquie Y, Lowman HB. Total alanine-scanning mutagenesis of insulin-like growth factor I (IGF-I) identifies differential binding epitopes for IGFBP-1 and IGFBP-3. Biochemistry 1999;38(20):6386-6396.
18. Zeslawski W, Beisel HG, Kamionka M, Kalus W, Engh RA, Huber R et al. The interaction of insulin-like growth factor-I with the N-terminal domain of IGFBP-5. EMBO J 2001;20(14):3638-3644.

19. Headey SJ, Keizer DW, Yao S, Wallace JC, Bach LA, Norton RS. Binding site for the C-domain of insulin-like growth factor (IGF) binding protein-6 on IGF-II; implications for inhibition of IGF actions. FEBS Lett 2004;568(1-3):19-22.
20. Hodgson DR, May FE, Westley BR. Mutations at positions 11 and 60 of insulin-like growth factor 1 reveal differences between its interactions with the type I insulin-like-growth-factor receptor and the insulin receptor. Eur J Biochem 1995;233(1):299-309.
21. Maly P, Luthi C. The binding sites of insulin-like growth factor I (IGF I) to type I IGF receptor and to a monoclonal antibody. Mapping by chemical modification of tyrosine residues. J Biol Chem 1988;263(15):7068-7072.
22. Cascieri MA, Chicchi GG, Applebaum J, Hayes NS, Green BG, Bayne ML. Mutants of human insulin-like growth factor I with reduced affinity for the type 1 insulin-like growth factor receptor. Biochemistry 1988;27(9):3229-3233.
23. Shooter GK, Magee B, Soos MA, Francis GL, Siddle K, Wallace JC. Insulin-like growth factor (IGF)-I A- and B-domain analogues with altered type 1 IGF and insulin receptor binding specificities. J Mol Endocrinol 1996;17(3):237-246.
24. Cascieri MA, Chicchi GG, Applebaum J, Green BG, Hayes NS, Bayne ML. Structural analogs of human insulin-like growth factor (IGF) I with altered affinity for type 2 IGF receptors. J Biol Chem 1989;264(4):2199-2202.
25. Jansson M, Andersson G, Uhlen M, Nilsson B, Kordel J. The insulin-like growth factor (IGF)binding protein 1 binding epitope on IGF-I probed by heteronuclear NMR spectroscopy and mutational analysis. J Biol Chem 1998;273(38):24701-24707.
26. McRory JE, Sherwood NM. Catfish express two forms of insulin-like growth factor-I (IGF-I) in the brain. Ubiquitous IGF-I and brain-specific IGF-I. J Biol Chem 1994;269(28):18588-18592.
27. Sakano K, Enjoh T, Numata F, Fujiwara H, Marumoto Y, Higashihashi N et al. The design, expression, and characterization of human insulin-like growth factor II (IGF-II) mutants specific for either the IGF-II/cation-independent mannose 6-phosphate receptor or IGF-I receptor. J Biol Chem 1991;266(31):20626-20635.
28. Nanjo K, Sanke T, Miyano M, Okai K, Sowa R, Kondo M et al. Diabetes due to secretion of a structurally abnormal insulin (insulin Wakayama). Clinical and functional characteristics of [LeuA3] insulin. J Clin Invest 1986;77(2):514-519.
29. Nanjo K, Miyano M, Kondo M, Sanke T, Nishimura S, Miyamura K et al. Insulin Wakayama: familial mutant insulin syndrome in Japan. Diabetologia 1987;30(2):87-92.
30. Hua QX, Hu SQ, Frank BH, Jia W, Chu YC, Wang SH et al. Mapping the functional surface of insulin by design: structure and function of a novel A-chain analogue. J Mol Biol 1996;264(2):390-403.
31. Hua QX, Shoelson SE, Kochoyan M, Weiss MA. Receptor binding redefined by a structural switch in a mutant human insulin. Nature 1991;354(6350):238-241.
32. Xu B, Hua QX, Nakagawa SH, Jia W, Chu YC, Katsoyannis PG et al. Chiral mutagenesis of insulin's hidden receptor-binding surface: structure of an allo-isoleucine(A2) analogue. J Mol Biol 2002;316(3):435-441.
33. Wan ZL, Xu B, Chu YC, Katsoyannis PG, Weiss MA. Crystal structure of allo-Ile(A2)-insulin, an inactive chiral analogue: implications for the mechanism of receptor binding. Biochemistry 2003;42(44):12770-12783.
34. Xu B, Hu SQ, Chu YC, Huang K, Nakagawa SH, Whittaker J et al. Diabetes-associated mutations in insulin: consecutive residues in the B chain contact distinct domains of the insulin receptor. Biochemistry 2004;43(26):8356-8372.

35. Xu B, Hu SQ, Chu YC, Wang S, Wang RY, Nakagawa SH et al. Diabetes-associated mutations in insulin identify invariant receptor contacts. Diabetes 2004;53(6):1599-1602.
36. Kobayashi M, Takata Y, Ishibashi O, Sasaoka T, Iwasaki TM, Shigeta Y et al. Receptor binding and negative cooperativity of a mutant insulin, [LeuA3]-insulin. Biochem Biophys Res Commun 1986;137(1):250-257.
37. Nakagawa SH, Tager HS. Importance of aliphatic side-chain structure at positions 2 and 3 of the insulin A chain in insulin-receptor interactions. Biochemistry 1992;31(12):3204-3214.
38. Chen H, Feng YM. Hydrophilic Thr can replace the hydrophobic and absolutely conservative A3Val in insulin. Biochim Biophys Acta 1998;1429(1):69-73.
39. Olsen HB, Ludvigsen S, Kaarsholm NC. The relationship between insulin bioactivity and structure in the NH2-terminal A-chain helix. J Mol Biol 1998;284(2):477-488.
40. Xu B, Hua QX, Nakagawa SH, Jia W, Chu YC, Katsoyannis PG et al. A cavity-forming mutation in insulin induces segmental unfolding of a surrounding alpha-helix. Protein Sci 2002;11(1):104-116.
41. Horovitz A, Matthews JM, Fersht AR. Alpha-helix stability in proteins. II. Factors that influence stability at an internal position. J Mol Biol 1992;227(2):560-568.
42. Blaber M, Zhang XJ, Matthews BW. Structural basis of amino acid alpha helix propensity. Science 1993;260(5114):1637-1640.
43. Jonson PH, Petersen SB. A critical view on conservative mutations. Protein Eng 2001;14(6):397-402.
44. Pietrzkowski Z, Lammers R, Carpenter G, Soderquist AM, Limardo M, Phillips PD et al. Constitutive expression of insulin-like growth factor 1 and insulin-like growth factor 1 receptor abrogates all requirements for exogenous growth factors. Cell Growth Differ 1992;3(4):199-205.
45. Sell C, Dumenil G, Deveaud C, Miura M, Coppola D, DeAngelis T et al. Effect of a null mutation of the insulin-like growth factor I receptor gene on growth and transformation of mouse embryo fibroblasts. Mol Cell Biol 1994;14(6):3604-3612.
46. King R, Wells JR, Krieg P, Snoswell M, Brazier J, Bagley CJ et al. Production and characterization of recombinant insulin-like growth factor-I (IGF-I) and potent analogues of IGF-I, with Gly or Arg substituted for Glu3, following their expression in Escherichia coli as fusion proteins. J Mol Endocrinol 1992;8(1):29-41.
47. Torres AM, Forbes BE, Aplin SE, Wallace JC, Francis GL, Norton RS. Solution structure of human insulin-like growth factor II. Relationship to receptor and binding protein interactions. J Mol Biol 1995;248(2):385-401.
48. Milner SJ, Francis GL, Wallace JC, Magee BA, Ballard FJ. Mutations in the B-domain of insulin-like growth factor-I influence the oxidative folding to yield products with modified biological properties. Biochem J 1995;308(Pt 3):865-871.
49. Mazor O, Hillairet dB, Lombet A, Gruaz-Guyon A, Gayer B, Skrzydelsky D et al. Europium-labeled epidermal growth factor and neurotensin: novel probes for receptor-binding studies. Anal Biochem 2002;301(1):75-81.
50. Soos MA, O'Brien RM, Brindle NP, Stigter JM, Okamoto AK, Whittaker J et al. Monoclonal antibodies to the insulin receptor mimic metabolic effects of insulin but do not stimulate receptor autophosphorylation in transfected NIH 3T3 fibroblasts. Proc Natl Acad Sci U S A 1989;86(14):5217-5221.
51. Soos MA, Field CE, Lammers R, Ullrich A, Zhang B, Roth RA et al. A panel of monoclonal antibodies for the type I insulin-like growth factor receptor. Epitope mapping, effects on ligand binding, and biological activity. J Biol Chem 1992;267(18):12955-12963.

52. Ouwens DM, van der Zon GC, Pronk GJ, Bos JL, Moller W, Cheatham B et al. A mutant insulin receptor induces formation of a Shc-growth factor receptor bound protein 2 (Grb2) complex and p21ras-GTP without detectable interaction of insulin receptor substrate 1 (IRS1) with Grb2. Evidence for IRS1-independent p21ras-GTP formation. J Biol Chem 1994;269(52):33116-33122.
53. Kamp GA, Ouwens DM, Hoogerbrugge CM, Zwinderman AH, Maassen JA, Wit JM. Skin fibroblasts of children with idiopathic short stature show an increased mitogenic response to IGF-I and secrete more IGFBP-3. Clin Endocrinol (Oxf) 2002;56(4):439-447.
54. Lofas S, Johnsson B. A novel hydrogel matrix on gold surfaces in surface plasmon resonance sensors for fast and efficient covalent immobilization of ligands. J Chem Soc Chem Commun 1990;211526-1528.
55. Carrick FE, Forbes BE, Wallace JC. BIAcore analysis of bovine insulin-like growth factor (IGF)-binding protein-2 identifies major IGF binding site determinants in both the amino- and carboxyl-terminal domains. J Biol Chem 2001;276(29):27120-27128.
56. Forbes BE, Hartfield PJ, McNeil KA, Surinya KH, Milner SJ, Cosgrove LJ et al. Characteristics of binding of insulin-like growth factor (IGF)-I and IGF-II analogues to the type 1 IGF receptor determined by BIAcore analysis. Eur J Biochem 2002;269(3):961-968.
57. Hobba GD, Lothgren A, Holmberg E, Forbes BE, Francis GL, Wallace JC. Alanine screening mutagenesis establishes tyrosine 60 of bovine insulin-like growth factor binding protein-2 as a determinant of insulin-like growth factor binding. J Biol Chem 1998;273(31):19691-19698.
58. Wong MS, Fong CC, Yang M. Biosensor measurement of the interaction kinetics between insulin-like growth factors and their binding proteins. Biochim Biophys Acta 1999;1432(2):293-301.
59. Heding A, Gill R, Ogawa Y, De Meyts P, Shymko RM. Biosensor measurement of the binding of insulin-like growth factors I and II and their analogues to the insulin-like growth factor-binding protein-3. J Biol Chem 1996;271(24):13948-13952.
60. Marinaro JA, Jamieson GP, Hogarth PM, Bach LA. Differential dissociation kinetics explain the binding preference of insulin-like growth factor binding protein-6 for insulin-like growth factor-II over insulin-like growth factor-I. FEBS Lett 1999;450(3):240-244.
61. Sklenar V, Peterson RD, Rejante MR, Feigon J. Two- and three-dimensional HCN experiments for correlating base and sugar resonances in 15N,13C-labeled RNA oligonucleotides. J Biomol NMR 1993;3(6):721-727.
62. Bartels C, Xia TH, Billeter M, Guntert P, Wuthrich K. The program XEASY for computer-supported NMR spectral analysis of biological macromolecules. J Biomol NMR 1995;51-10.
63. Wishart DS, Bigam CG, Yao J, Abildgaard F, Dyson HJ, Oldfield E et al. 1H, 13C and 15N chemical shift referencing in biomolecular NMR. J Biomol NMR 1995;6(2):135-140.
64. Mandel AM, Akke M, Palmer AG, III. Backbone dynamics of Escherichia coli ribonuclease HI: correlations with structure and function in an active enzyme. J Mol Biol 1995;246(1):144-163.
65. Farrow NA, Muhandiram R, Singer AU, Pascal SM, Kay CM, Gish G et al. Backbone dynamics of a free and phosphopeptide-complexed Src homology 2 domain studied by 15N NMR relaxation. Biochemistry 1994;33(19):5984-6003.
66. Farmer BT, Constantine KL, Goldfarb V, Friedrichs MS, Wittekind M, Yanchunas J, Jr. et al. Localizing the NADP+ binding site on the MurB enzyme by NMR. Nat Struct Biol 1996;3(12):995-997.
67. Perdue JF, Bach LA, Hashimoto R et al. Structural determinants for the binding of insulin-like growth factor-II to IGF and insulin receptors and binding proteins. In: Baxter RC, Gluckman PD, Rosenfeld RG, editors. The insulin-like growth factors and their regulatory proteins. New York: Elsevier, 1994:67-76.

Supplemental data

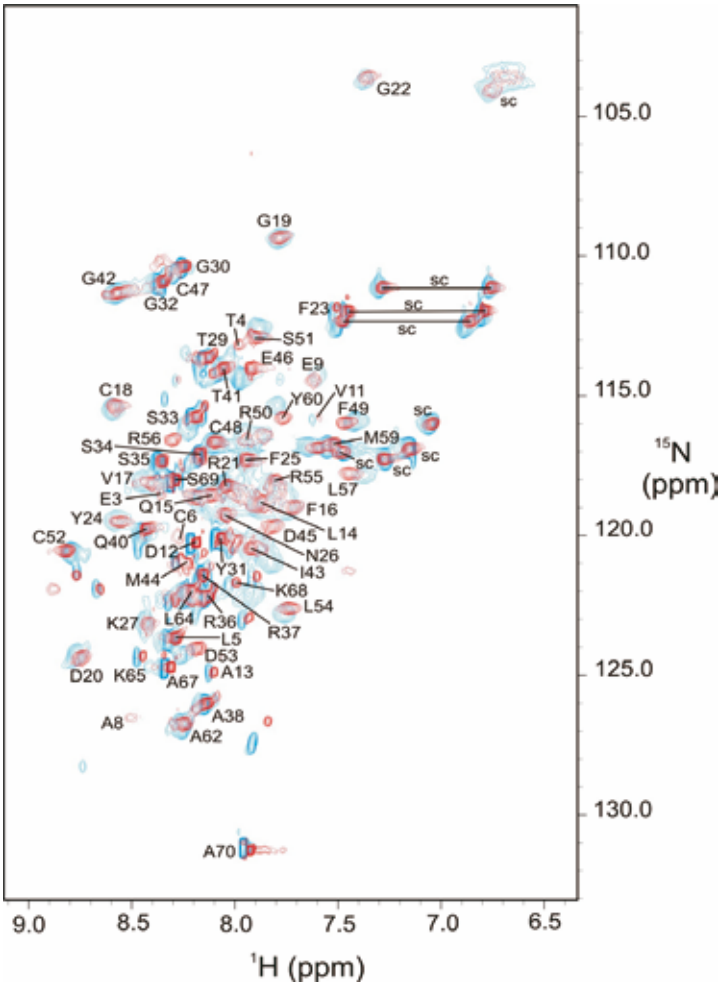

Figure S1. Contour plots of 600 MHz 2D ^{1}H-^{15}N-HSQC spectra with V44M IGF-I in red and native IGF-I in blue. The V44M IGF-I spectrum was acquired using a 0.9 mM sample at 37 °C and pH 5.1 in 95% H2O/5% $^{2}H_2O$ containing 10mM acetate- $^{2}H_4$ and 0.02% sodium azide, while the IGF-I spectrum was acquired on a 0.5 mM sample at 37°C and pH 4.9 in 95% H2O/5% $^{2}H_2O$ containing 10mM sodium acetate. Resonances are labelled with the corresponding sequence positions and side-chain amide resonances (Asn and Gln) are connected with a line. Other side chain resonances are labelled with a "sc" sign. Unlabelled peaks are not assigned.

Table S1. Residues showing significant differences in ^{1}H and ^{15}N chemical shifts ($\Delta\delta_{av}$>0.3) between V44M IGF-I and IGF-I plus F1 peptide (8), where $\Delta\delta_{av}=(\Delta\delta_{NH}^{2}+0.17\Delta\delta_{N}^{2})^{1/2}$ (66). Chemical shifts for these residues in long-[Arg3] IGF-I (10) and long-[Leu60] IGF-I (11) are also included. The residues implicated in F1 peptide binding actions (8) are shown in black and others shaded in gray.

residue	V44M IGF-I		IGF-I plus F1		Long-[Arg3]IGF-I		Long-[Leu60] IGF-I	
	NH	N	NH	N	NH	N	NH	N
Cys 6	8.25	120.2	8.47	118.0	8.38	119.7	8.33	118.3
Gly7*	-------	-------	8.86	109.7	7.74	110.0	7.63	108.3#
Ala8*	8.49	126.5	8.77	128.5	8.98	130.3	8.83	128.2
Glu9	7.61	114.5	7.80	115.5	8.00	118.1	7.94	115.1#
Leu10*	-------	-------	6.74	119.9	6.88	121.7	6.87	120.3
Val11	7.59	115.7	7.18	118.1	7.29	119.3	7.38	117.9
Phe16	7.71	119.0	8.29	121.2	7.84	120.6	7.38	117.9#
Phe25	7.93	117.3	8.53	116.9	8.48	119.6	7.86	120.3#
Ile43	7.91	120.4	7.58	121.5	7.89	122.4	7.74	121.4
Phe49	7.45	115.9	7.70	116.1	7.72	117.3	7.89	113.7#
Arg50	7.93	116.5	7.42	117.1	7.53	119.9	7.95	119.4
Ser51	7.90	112.9	7.75	110.7	7.83	113.3	7.81	112.9
Leu54	7.73	122.6	8.67	127.0	7.59	123.6	7.57	122.5#
Arg55	7.80	118.0	8.22	117.5	7.86	119.9	7.92	119.4
Glu58*	-------	-------	7.40	112.5	8.09	114.8	8.15	113.7
Tyr60	7.76	115.8	7.81	117.5	7.98	117.0	7.76	117.9
Cys61*	-------	-------	7.09		7.26	116.9	7.22	115.3

* Gly7, Leu10, Glu58 and Cys61 are not found in any spectra of 15°C, 20°C and 37°C in V44M IGF-I.
+ Ala8 has a very weak peak in 2D HSQC.
# Chemical shifts show significant differences among the three published IGF-I data sets.

Table S2. NOE intensities observed in Val44Met IGF-I compared with inter-proton distances for the mutated residue 44 in A) long-[Arg3] IGF-I (12) and B) IGF-I plus F1 peptide (8). Relative intensities (RI), calculated using the integrated intensity divided by the average noise in the 3D NOESY-HSQC spectrum, are designated S (strong, RI>3.5), M (medium, 3.5>RI>2.0) and W (weak, RI<2.0). HN-HN and HN-HA NOEs and corresponding distances are shaded in grey. Note that the relative strengths of the sequential NOEs to Met44 HN correspond more closely with the distances in the long-[Arg3] IGF-I structure. Several backbone-to-backbone NOEs expected from the long-[Arg3] IGF-I structure are not seen in spectra of Val44Met IGF-I as follows: HN of Asn26, Gly42, Glu46, Cys47, Cys48 to Met44 HN; HN of Leu10, Val11, Glu46, Cys47, Cys48 to Met44 H^{α}. NOEs expected from the IGF-I+F1 structure but not seen in spectra of Val44Met IGF-I are: HN of Gly42, Glu46, Cys47, Cys48 to Met44 HN; HN of Glu46, Cys47, Cys48, Phe49 to Met44 H^{α}. However, a number of these expected NOEs are also not observed in our spectra of native IGF-I, probably as a result of the effects of conformational averaging and aggregation.

A.		NOEs observed in 3D ^{1}H-^{15}N-NOESY-HSQC spectrum of V44M IGF-I				Inter-proton distances in the native IGF-I structure (Å) for pairwise interactions giving rise to NOEs in the spectrum of Val44Met			
		Met44				**Val44**			
		HN	HA	HB	HG21	HN	HA	HB	HG21
Ile43	HN	W		W		2.55-2.84		5.55-5.96	
	HA	M				3.34-3.45			
	HG23	S				3.49-4.93			
Asp45	HN	S	S	S		1.90-2.18	3.59-3.63	2.79-3.18	
Thr41	HN				M				6.62-9.09

B.		NOEs observed in 3D ^{1}H-^{15}N-NOESY-HSQC spectrum of V44M IGF-I				Inter-proton distances in the native IGF-I structure (Å) for pairwise interactions giving rise to NOEs in the spectrum of Val44Met			
		Met44				**Val44**			
		HN	HA	HB	HG21	HN	HA	HB	HG21
Ile43	HN	W		W		2.06-2.71		4.23-4.94	
	HA	M				3.49-3.57			
	HG23	S				2.48-3.96			
Asp45	HN	S	S	S		2.76-2.99	3.57-3.59	3.53-3.73	
Thr41	HN				M				7.13-9.92

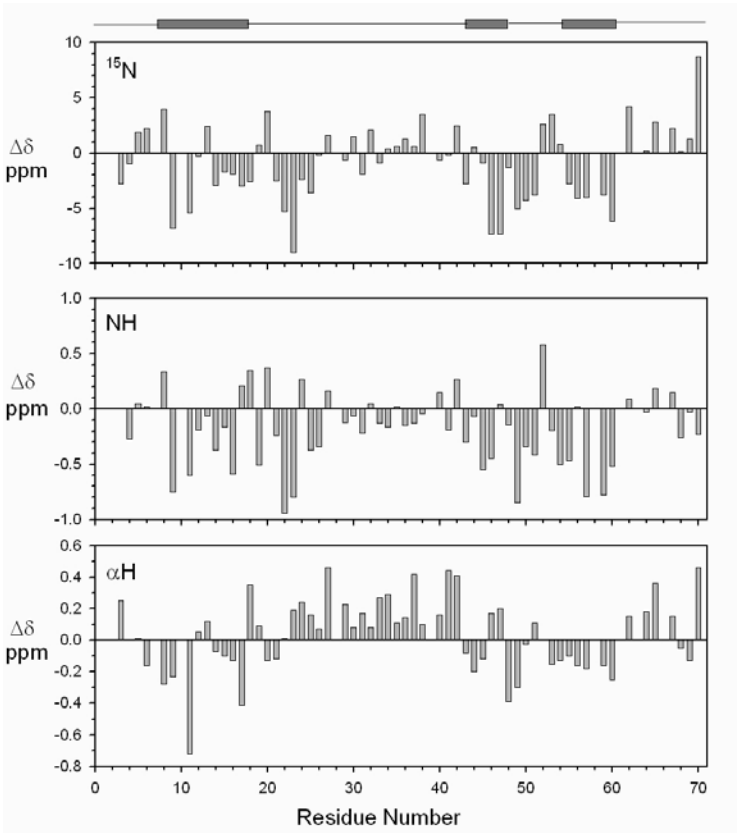

Figure S2. Deviations from random coil chemical shifts for ^{15}N, NH and H^{α} resonances in Val44Met IGF-I. Random coil values were taking from published data (16). Residues Gly1, Gly7, Leu10, Glu58 and Cys61 were not assigned. Residues 2, 28, 39, 63 and 66 are proline and the other gaps are calculated to be zero. The locations of the three helices of native IGF-I are indicated above the plot.

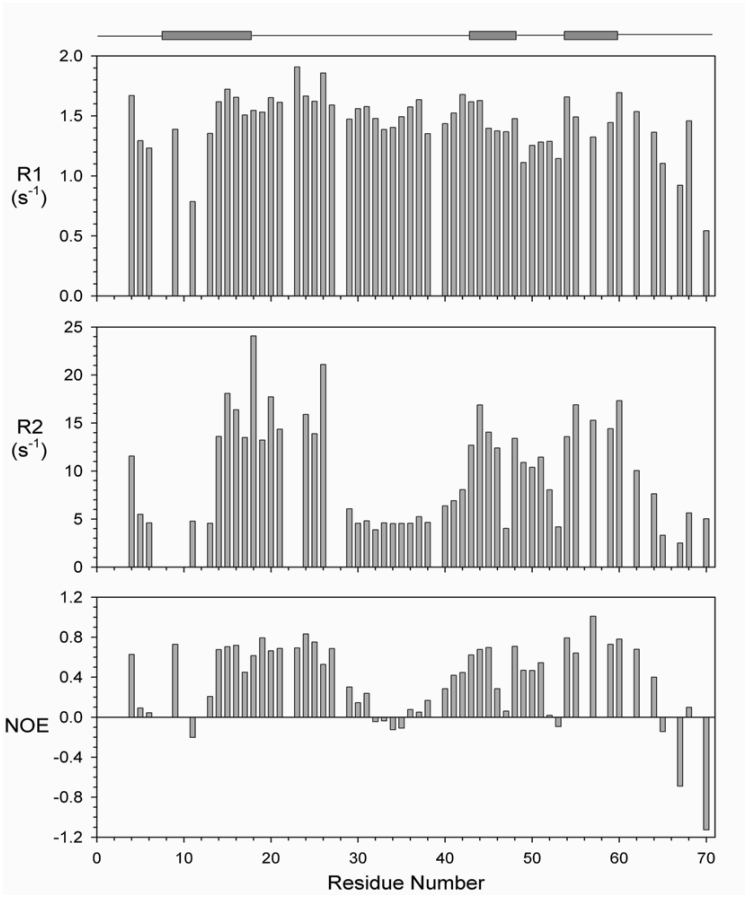

Figure S3. Summary of 15N backbone relaxation parameters R1, R2 and steady-state 1H-15N NOE for V44M IGF-I. Residues Gly1, Gly7, Leu10, Glu58 and Cys61 were not assigned. Residues Glu3, Ala8, Asp12, Gly22, Arg56 and Ser69 are not shown due to poor fitting and overlap. Residues Glu9, Phe23 and Lys27 are not shown in the R2 plot because of their very short T2 values. Residues 2, 28, 39, 63 and 66 are proline. The locations of the three helices of native IGF-I are indicated above the plot.